Can Nanocavities Significantly Enhance Resonance Energy Transfer in a Single Donor-Acceptor Pair?

*Yu-Chen Wei,[a,b] Ming-Wei Lee,[a] Pi-Tai Chou,[b] Gregory D. Scholes,[c] George C. Schatz,[d] Liang-Yan Hsu [a]**

[a]Institute of Atomic and Molecular Sciences, Academia Sinica, Taipei 10617, Taiwan

[b]Department of Chemistry, National Taiwan University, Taipei, 10617 Taiwan, R.O.C.

[c]Department of Chemistry, Frick Chemistry Laboratory, Princeton University, Princeton, New Jersey 08544, United States

[d]Department of Chemistry, Northwestern University, Evanston, Illinois 60208, United States

*Liang-Yan Hsu. Email: lyhsu@gate.sinica.edu.tw

Abstract

Long-range resonance energy transfer (RET) and controlling energy transfer at the nanoscale have received considerable attention both experimentally and theoretically during the past few decades. We have investigated RET between a donor/acceptor pair in the nanocavities based on our previous theory developed in the framework of macroscopic quantum electrodynamics (QED). Based on this theory, the enhancements in RET with respect to the rate in vacuum were evaluated for a Fabry–Pérot (FP) cavity. When the displacement vector between the two molecules is aligned with the cavity axis of the Fabry–Pérot cavity, we found that cavity modes give less than a factor of 10 enhancements due to the interference between contributions from resonant and non-resonant cavity modes. By comparison, when the displacement vector between the two molecules is aligned in a plane perpendicular to the cavity axis, we found that the cavity modes can induce enhancements over a factor of 10, and the surface plasmon polariton modes can induce enhancements up to a factor of 300. We develop a convenient representation for understanding the effect of the displacement vector between the molecules, and of the molecular dipole directions in terms of H-dimer and J-dimer properties. To further enhance RET, we propose a square silver cavity that gives a factor of 280 rate enhancement under cavity resonance conditions, which provides important insight for developing devices capable of long-range RET.

1. Introduction

Resonant energy transfer (RET) at the nanoscale plays a key role in light harvesting,[1-7] photovoltaics,[8-10] surface enhanced Raman spectroscopy[11-12] and molecular biosensing.[13-14] Due to these important applications, RET and dipole-dipole interactions have attracted extensive interest, and the enhancement and manipulation of long-range RET rates have become crucial issues in physical chemistry.[15-21] During the past decade, it has been reported that long-range RET rates could be modified through the design of the dielectric environments including metal surfaces,[22-23] nanoparticles[24-26], cavities[26-29] and other dimensionally constrained nanostructures.[30-34] Among these dielectric environments, many studies have an emphasis on cavities owing to their tunable resonance frequency and convenient preparation. In 2000, Barnes et.al. demonstrated that the energy transfer rate depends linearly on the donor emission rate and hence photonic mode

density.[35] Recently, the distance independence of RET rates up to 100 nm has been observed in Fabry–Pérot (FP) cavities with significant light-matter coupling.[36] In addition, RET rates in cavities up to 7 times higher than those in vacuum have been observed.[37] These studies believe that the strongest RET occurs along the cavity axis (the normal direction of cavity surfaces) without clear evidence. To investigate the mechanism of the phenomena, several theories covering cavity-mediated energy transfer and polariton-assisted remote energy transfer have been developed.[38-41] In these theories, two important assumptions are made: the consideration of a single photonic mode and phenomenological dissipation rates. However, the validities of the assumptions have not been carefully examined. In addition to the single mode model, some theories started from molecular quantum electrodynamics and applied the perturbation expansion in a vacuum photon basis to evaluate the coupling of RET.[18, 20, 41-43] Nonetheless, when free electromagnetic fields are strongly coupled to a dielectric environment, the perturbation approach may not be valid under such a basis.

In fact, without applying the two assumptions above or incorporating high-order perturbation terms, the RET rate can be evaluated within the framework of macroscopic quantum electrodynamics (QED). Macroscopic QED enables us to resolve the linear response of photon dressed by medium polarization (polariton) from external sources, e.g., a dipole source.[44-52] The development of macroscopic QED can be traced back to the middle of the twentieth century,[53-54] but no significant progress has been made until Huttner and Barnett's breakthrough in 1992.[55] Huttner and Barnett established a theoretical framework by incorporating an absorptive dielectric environment into the Hopfield model.[56] After that, Welsch et al. further extended the Huttner-Barnett model and connected field operators and macroscopic Maxwell's equations via dyadic Green's functions.[57] In this framework, photon dressed by medium polarization can be precisely described. Through this approach, we have investigated the enhancements in RET coupled with surface plasmons in bulk metal, a metal thin film and a metal nanosphere, characterizing the spatial dependence of the RET enhancement.[58-62] Moreover, Wenger et. al utilized a similar approach to analyze rate enhancements for RET in the microwave regime, showing consistency between analytical solutions and experimental results in cavities.[28] Under a nearly lossless cavity, the strongest rate enhancements measured were around 4 fold at $kR > 0.7$ where k is the wavevector of the propagated light and R is the donor/acceptor distance.[29] Similar order of magnitude of the

RET enhancement was also observed in the FP nanocavity.[63] Such weak rate enhancements imply that the FP cavity may not be able to enhance RET rates as intuitively thought.

In this study, we focus on whether RET can be enhanced in a nanocavity. In order to clarify the validities of the assumptions in the previous studies,[38-40] we consider a realistic cavity, which resembles a dielectric environment used in the experiments.[36-37] To evaluate the RET rates, we use the macroscopic QED approach which allows us to incorporate the effects of dielectric environments and all the degrees of freedom of photonic modes (both resonant and non-resonant) into the simulation. The advantage of the present approach is that all variables can be obtained from experiments or ab initio calculations, i.e., no free parameter. For example, dielectric functions in our theory can be measured through reflection and transmission measurements[64-65] or calculated by density functional theory.[66-67] In addition, the results enable us to clarify issues related to weak RET enhancements in nanocavities.

This article is organized as follows. Section 2.1 introduces the formalisms of RET based on the macroscopic QED approach. According to the formalisms, we need to evaluate the electric field in nanocavities, which is calculated by the Finite-Difference Time-Domain (FDTD) method introduced in Section 2.2. In Section 3.1, to verify a long-standing physical picture of RET in cavities,[36-40, 68] we compare the RET enhancements in the perfect FP cavity and those in the silver FP cavity where the donor is located at the center. In Section 3.2, to clarify how the cavity loss influences RET processes, we investigate the metal thickness dependence on the RET enhancements in the silver FP cavity. In Section 3.3, considering the reality that molecules are distributed in a cavity, we explore the position dependence of the donor on the RET enhancements. Moreover, according to the displacement vector and dipole alignments of the donor and acceptor, we summarize different types of RET enhancements in a silver FP cavity, which provides key insights into exploring RET, dipole-dipole interaction, and polariton chemistry in nanocavities. In Section 3.4, to demonstrate how to manipulate RET via material structure designs, we propose a square silver cavity with remarkable RET enhancements. In Section 4, we summarize the above results and discuss the significance of this work and future perspectives of the long-range RET.

2. Methods

2.1. Formalisms of RET

We applied a general theory of RET based on macroscopic QED,[44, 46-48, 58, 61] which considers retardation and the dielectric properties of materials in determining energy transfer rates. Note that this theory is not limited to RET coupled with plasmons, and it can be applied to RET in the presence of dielectric environments with any space-dependent, frequency-dependent, or complex dielectric functions. We emphasize this advantage because the scope of our theory was misunderstood by some literature.[16] In other words, this theory can include cavity modes and plasmon polariton modes together. According to this theory, RET rates k_{ET} can be evaluated in terms of the absorption line shape of the acceptor molecule $W_{\mathrm{abs}}(\bar{\upsilon})$ and the emission line shape of the donor molecule $W_{\mathrm{em}}(\bar{\upsilon})$,[15, 69]

$$\begin{aligned} k_{\mathrm{ET}} &= \frac{\hbar}{2\pi}\int dE W_{\mathrm{em}}\left(E\right)W_{\mathrm{abs}}\left(E\right)F\left(\mathbf{r}_{\mathrm{D}},\mathbf{r}_{\mathrm{A}},E\right) \\ &= \hbar^2 c\int d\bar{\upsilon} W_{\mathrm{em}}\left(\bar{\upsilon}\right)W_{\mathrm{abs}}\left(\bar{\upsilon}\right)F\left(\mathbf{r}_{\mathrm{D}},\mathbf{r}_{\mathrm{A}},\bar{\upsilon}\right) \end{aligned} \tag{1}$$

where

$$\begin{aligned} W_{\mathrm{em}}\left(\bar{\upsilon}\right) &= \frac{1}{\hbar^2 c}\sum_{d,d'} P_d \left|\mathbf{p}_{\mathrm{D}}\right|^2 \left|\left\langle \phi_{d'} \middle| \phi_d \right\rangle\right|^2 \delta\left(\bar{\upsilon}_{d'} - \bar{\upsilon}_d - \bar{\upsilon}\right) \\ W_{\mathrm{abs}}\left(\bar{\upsilon}\right) &= \frac{1}{\hbar^2 c}\sum_{a,a'} P_a \left|\mathbf{p}_{\mathrm{A}}\right|^2 \left|\left\langle \phi_{a'} \middle| \phi_a \right\rangle\right|^2 \delta\left(\bar{\upsilon}_{a'} - \bar{\upsilon}_a - \bar{\upsilon}\right) \end{aligned} \tag{2}$$

Here *d*' and *a*' (*d* and *a*) indicate the vibrational modes associated with the electronic excited (ground) state of donor and acceptor molecules, respectively. $|\langle\phi_{\mathrm{d}}|\phi_{\mathrm{d}'}\rangle|^2$ ($|\langle\phi_{\mathrm{a}'}|\phi_{\mathrm{a}}\rangle|^2$) denotes the Franck−Condon factor of a donor (acceptor) molecule. P_{d} (P_{a}) corresponds to the probability distribution of donor (acceptor) molecules at thermal equilibrium. $\mathbf{p}_{\mathrm{D}}$ ($\mathbf{p}_{\mathrm{A}}$) represents the transition dipole of a donor (acceptor) molecule. $F(\mathbf{r}_{\mathrm{D}}, \mathbf{r}_{\mathrm{A}}, \bar{\upsilon})$ is the electromagnetic coupling factor in wavenumber units. $\mathbf{r}_{\mathrm{D}}$ and $\mathbf{r}_{\mathrm{A}}$ denote the positions of a donor and an acceptor, respectively. The concept of the coupling factor $F(\mathbf{r}_{\mathrm{D}}, \mathbf{r}_{\mathrm{A}}, \bar{\upsilon})$ is not the same as that of $|\mathrm{sV_s}|^2$ in Ref. [6] (or related

concepts from other literature),[7, 70] where s is a factor due to the solvent medium that screens the direct coupling V_s. The coupling factor is given by eq 3.

$$F\left(\mathbf{r}_{\mathrm{D}},\mathbf{r}_{\mathrm{A}},\bar{\upsilon}\right)=\left|\frac{\hat{\mathbf{e}}_{\mathrm{A}}\cdot\mathbf{E}^{\mathrm{D}}\left(\mathbf{r}_{\mathrm{D}},\mathbf{r}_{\mathrm{A}},\bar{\upsilon}\right)}{\mathrm{p}_{\mathrm{D}}\left(\bar{\upsilon}\right)}\right|^{2} \tag{3}$$

where $\hat{\mathbf{e}}_{\mathrm{A}}$ specifies the transition dipole orientation of the acceptor chromophore, and $\mathbf{E}^{\mathrm{D}}(\mathbf{r}_{\mathrm{D}}, \mathbf{r}_{\mathrm{A}}, \bar{\upsilon})$ indicates the electric field at $\mathbf{r}_{\mathrm{A}}$ generated by the donor chromophore at $\mathbf{r}_{\mathrm{D}}$ with the transition dipole moment $\mathbf{p}_{\mathrm{D}}(\bar{\upsilon}) = \mathrm{p}_{\mathrm{D}}(\bar{\upsilon})\hat{\mathbf{e}}_{\mathrm{D}}$. Note that the donor (acceptor) chromophore is approximated as a point dipole in this theory. In addition, the coupling factor F does not correspond to the spectral density of photons, which is associated with single-point dyadic Green's function[48] (In fact, the pariton kernel of Eq. (10) in Ref. [48] corresponds to the spectral density of photons). Instead, the coupling factor corresponds to the two-point dyadic Green's function in a cavity. Based on the point dipole approximation, the electric field $\mathbf{E}^{\mathrm{D}}(\mathbf{r}_{\mathrm{D}}, \mathbf{r}_{\mathrm{A}}, \bar{\upsilon})$ can be solved analytically via the dyadic Green's function in Gaussian units.

$$\mathbf{E}^{\mathrm{D}}\left(\mathbf{r}_{\mathrm{D}},\mathbf{r}_{\mathrm{A}},\bar{\upsilon}\right)=16\pi^{3}\bar{\upsilon}^{2}\overline{\overline{\mathbf{G}}}\left(\mathbf{r}_{\mathrm{D}},\mathbf{r}_{\mathrm{A}},\bar{\upsilon}\right)\cdot\mathbf{p}_{\mathrm{D}}\left(\bar{\upsilon}\right) \tag{4}$$

The dyadic Green's function $\overline{\overline{\mathbf{G}}}(\mathbf{r}_{\mathrm{D}}, \mathbf{r}_{\mathrm{A}}, \bar{\upsilon})$ in eq 4 obeys the Maxwell equations

$$\left[4\pi^{2}\varepsilon_{\mathrm{r}}\left(\mathbf{r},\bar{\upsilon}\right)\bar{\upsilon}^{2}-\nabla\times\nabla\times\right]\overline{\overline{\mathbf{G}}}\left(\mathbf{r}_{\mathrm{D}},\mathbf{r}_{\mathrm{A}},\bar{\upsilon}\right)=-\mathbf{I}_{3}\delta\left(\mathbf{r}_{\mathrm{A}}-\mathbf{r}_{\mathrm{D}}\right) \tag{5}$$

where $\varepsilon_{\mathrm{r}}(\mathbf{r}, \bar{\upsilon})$ is the frequency-dependent dielectric function, $\mathbf{I}_3$ is a three-dimensional identity matrix, and $\delta(\mathbf{r}_{\mathrm{A}} - \mathbf{r}_{\mathrm{D}})$ is the three-dimensional Dirac delta function. Note that Eq (5) has been extensively used in the field of nano optics,[71] and it is different from the coupling tensor in some QED studies.[18] Under the operation of the Green's function, the coupling factor $F(\mathbf{r}_{\mathrm{D}}, \mathbf{r}_{\mathrm{A}}, \bar{\upsilon})$ can be viewed as involving photon propagation (whether a real photon or a virtual photon) from the position of the donor chromophore $\mathbf{r}_{\mathrm{D}}$ to the position of the acceptor chromophore $\mathbf{r}_{\mathrm{A}}$. In vacuum, the analytical solution of the dyadic Green's function $\overline{\overline{\mathbf{G}}}_0(\mathbf{r}_{\mathrm{D}}, \mathbf{r}_{\mathrm{A}}, \bar{\upsilon})$ is given by,[16, 72]

$$\left[\bar{\bar{\mathbf{G}}}_0\left(\mathbf{r}_\mathrm{D},\mathbf{r}_\mathrm{A},\bar{\upsilon}\right)\right]_{ij} = \mathrm{G}_{0,ij}\left(\mathbf{r}_\mathrm{D},\mathbf{r}_\mathrm{A},\bar{\upsilon}\right) = \frac{\mathrm{e}^{\mathrm{i}kR}}{4\pi k^2}\left[\left(\delta_{ij}-\hat{R}_i\hat{R}_j\right)\frac{k^2}{R}+\left(3\hat{R}_i\hat{R}_j-\delta_{ij}\right)\left(\frac{1}{R^3}-\frac{ik}{R^2}\right)\right] \quad (6)$$

where $\mathbf{r}_\mathrm{A}-\mathbf{r}_\mathrm{D} = R\cdot\hat{R}$ describes the displacement vector between the donor dipole and the acceptor dipole ($\hat{R}$ is the unit vector of $\mathbf{r}_\mathrm{A}-\mathbf{r}_\mathrm{D}$), $k = 2\pi\bar{\upsilon}$, and δ_{ij} is the Kronecker delta function. To analyze the RET enhancement or suppression induced by the dielectric environments, we define the theoretical enhancement factor ($\mathrm{EF_{th}}$) as the following,

$$\mathrm{EF_{th}} \equiv \frac{F\left(\mathbf{r}_\mathrm{D},\mathbf{r}_\mathrm{A},\bar{\upsilon}\right)}{F_\mathrm{vac}\left(\mathbf{r}_\mathrm{D},\mathbf{r}_\mathrm{A},\bar{\upsilon}\right)} \quad (7)$$

where F and F_vac indicate the coupling factor in the system and vacuum, respectively. Note that the definition of the experimental enhancement factor ($\mathrm{EF_{exp}}$) is different from $\mathrm{EF_{th}}$. The former is defined as

$$\mathrm{EF_{exp}} \equiv \frac{k_\mathrm{ET}}{k_\mathrm{ET,vac}} = \frac{\int d\bar{\upsilon} W_\mathrm{em}\left(\bar{\upsilon}\right)W_\mathrm{abs}\left(\bar{\upsilon}\right)F\left(\mathbf{r}_\mathrm{D},\mathbf{r}_\mathrm{A},\bar{\upsilon}\right)}{\int d\bar{\upsilon} W_\mathrm{em}\left(\bar{\upsilon}\right)W_\mathrm{abs}\left(\bar{\upsilon}\right)F_\mathrm{vac}\left(\mathbf{r}_\mathrm{D},\mathbf{r}_\mathrm{A},\bar{\upsilon}\right)} \quad (8)$$

where k_ET and $k_\mathrm{ET,vac}$ indicate the RET rates in the system and vacuum, respectively. The concept of $\mathrm{EF_{th}}$ is useful because it provides upper/lower bounds to the $\mathrm{EF_{exp}}$. The relationship between $\mathrm{EF_{th}}$ and $\mathrm{EF_{exp}}$ is listed as follows,

$$\mathrm{Min}\left[\mathrm{EF_{th}}\right] \le \mathrm{EF_{exp}} \le \mathrm{Max}\left[\mathrm{EF_{th}}\right] \quad (9)$$

where $\mathrm{Max}[\mathrm{EF_{th}}]$ ($\mathrm{Min}[\mathrm{EF_{th}}]$) indicates the maximum (minimum) of $\mathrm{EF_{th}}$. (Recall that $\mathrm{EF_{th}}$ is a function of the wavenumber $\bar{\upsilon}$). The mathematical proofs of eq 9 are shown in the Supporting Information. In this work, we focus on the behavior of $\mathrm{EF_{th}}$.

2.2. Finite-Difference Time-Domain (FDTD) Simulation

To solve for the electric field in complex dielectric environments, we apply the computational electromagnetic software (Lumerical FDTD Solutions)[73] based on the finite-difference time

domain (FDTD) method. Several different systems were considered in our study, whose geometry setup will be described in the results and discussion. Here we provide the general parameters and settings used in these calculations. All simulations were set to run for 200 fs at which point the fraction of power remaining in the simulation is less than 10^{-7}. All boundaries are set to be perfectly matched layers (PMLs). The donor molecule was approximated as an oscillating electric point dipole source with the wavelength ranging from 200 to 800 nm. The dielectric functions of silver from Johnson and Christy[64] and SiO_2 from Palik[65] were used for the silver plates and SiO_2 medium, respectively. We set the FDTD domain to be 3000 × 3000 × 2000 nm. A conformal mesh of 0.5 nm was applied on the region to a 500 × 500 × 500 nm covering the dipole source and the monitor range, while the outside mesh was chosen to be auto-nonuniform with a mesh accuracy of 4 (a setting in the Lumerical FDTD Solutions).

3. Results and Discussion

3.1. Comparison between the perfect cavity and the silver cavity

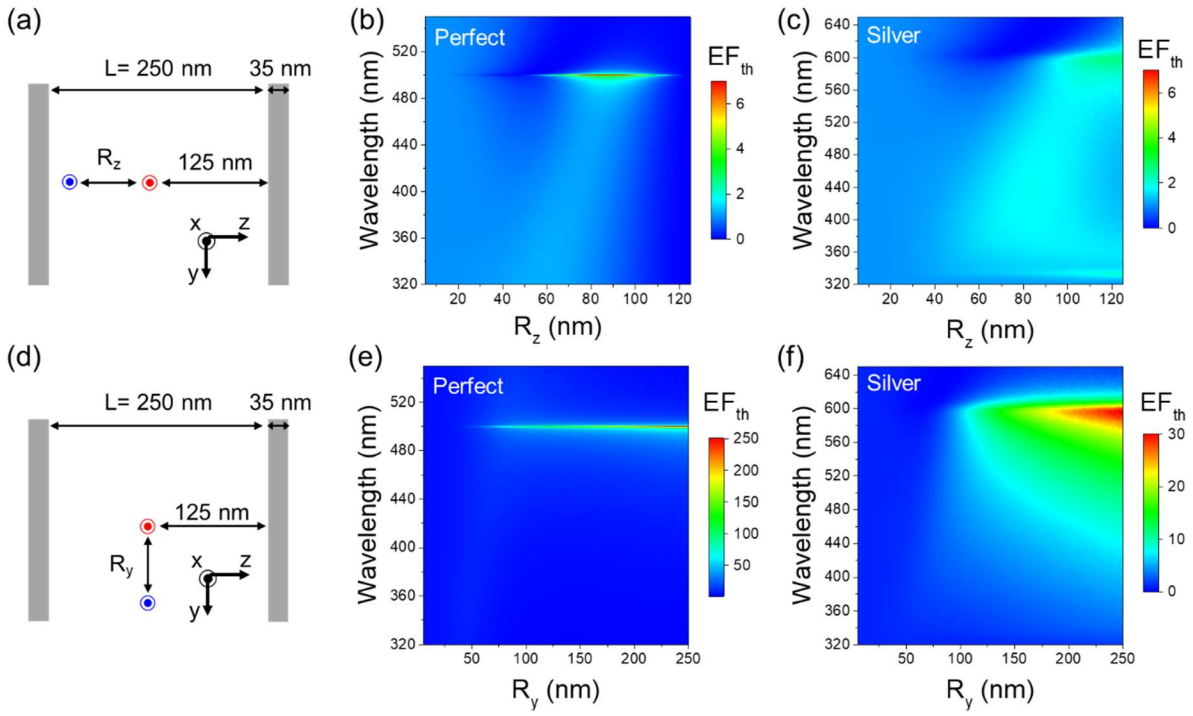

Figure 1. Theoretical RET enhancement (EF_{th}) in a FP cavity with the donor located at the center of the cavity. The FP cavity is made of two silver thin films (thickness=35 nm) separated by 250 nm. (a) The system with the donor (red) and the acceptor (blue) with the displacement (R_z) along the z direction. Both transition dipoles are along the x direction in (a) and (d). (b) and (c) show contours of the dependence of the enhancement factor for the perfect cavity and silver cavity, respectively, as a function of R_z and wavelength. (d) the system with the donor (red) and the acceptor (blue) with the displacement along the y direction (R_y). (e) and (f) show contours of the dependence of the enhancement factor for the perfect cavity and silver cavity, respectively, as a function of R_y and wavelength. Note that the vertical bars in (e) and (f) are distinct due to the one order of magnitude difference of EF_{th}.

To validate whether RET rates could be significantly enhanced by FP nanocavities and what their physical picture is, we analyze the RET enhancements in the perfect cavity and in the silver cavity. In this section, we would like to elaborate two important issues: First, for a single donor-acceptor pair along the cavity axis of a silver FP cavity, can RET be significantly enhanced by cavity modes? Second, is it appropriate to study RET in a realistic cavity by using the concept

of a perfect cavity? Here we started with a system in which the donor is located at the center of a FP cavity. The theoretical enhancement factors (EF_{th}) are calculated according to eqs 3-7. In **Figure 1a**, we set the cavity length L = 250 nm and the transition dipoles of donor and acceptor are oriented along the x direction (perpendicular to the cavity axis which corresponds to the z direction). Using the analytical solution of RET in the perfect cavity (without cavity loss),[68, 74] the EF_{th} were evaluated in **Figure 1b** as a function of the distance (R_z) in the z direction and of wavelength, showing that the resonance wavelength ($\lambda \approx 500$ nm) matches the wavelength of the lowest cavity mode. Due to the total reflection caused by the perfect cavity, divergence of the coupling factor (the singularity of the analytical solutions to the perfect cavity) occurs along $R_y = 0$ and the perfect cavity resonant condition ($\lambda = 500$ nm). Therefore, we plot the RET enhancement in the near-resonance situation under the constraint $R_y = 0.1$ nm, $\lambda \neq 500$ nm (we use $\lambda = 500.01$ and 499.24 nm instead) in **Figure 1b**. With this small wavelength shift ($\Delta\lambda \sim 0.01$ nm), the enhancement factor dramatically drops to around 9, i.e., the strong enhancement along the z direction only exists in a very narrow wavelength interval. More importantly, this indicates that it is difficult to use the cavity mode to enhance RET for this system. In addition, we found that significant suppression also occurs around the near-resonant wavelength. Such suppression together with a weak rate enhancement involving interference between the infinite intermediate electromagnetic states including the resonant cavity mode and non-resonant cavity modes, is summarized in **Scheme 1**. Here the terms "resonant" and "non-resonant" illustrate the energy alignments between the energy levels of donor/acceptor (degeneracy) and the intermediate states of the cavity. Moreover, interference between the two types of modes leads to wavelength dependence in the RET suppression (anti resonance) together with the strong RET enhancement (resonance) and an asymmetric Fano-like line shape, which has also been reported in the microwave regime.[29] Detailed derivations are shown in the Supporting Information. In brief, the pathways of energy transfer through the infinite non-resonant cavity modes are opposite in sign but similar order of magnitude in their contribution to the coupling factor compared with that involving the resonant cavity mode, leading to suppression and weak enhancement in RET (**Figure S1**). The numerical simulations and analytical solutions indicate that neglect of the infinite non-resonant cavity modes would lead to overestimation of the rate enhancement.

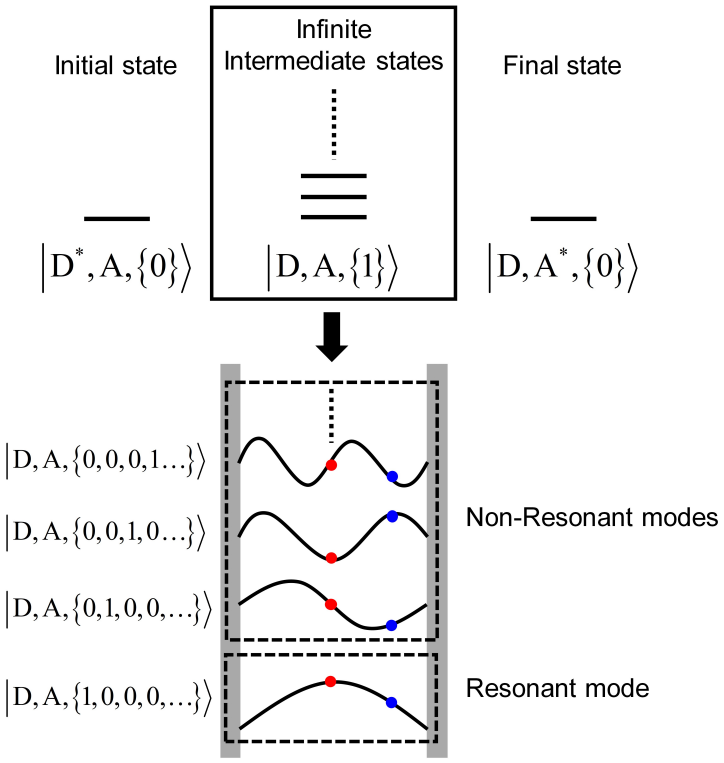

Scheme 1. Schematic illustration of RET through cavity modes in the FP cavity. D and A indicate the electronic ground states of the donor and acceptor, respectively. * denotes the excited electronic states. {0} and {1} are the sets of the cavity modes occupied by 0 and 1 photon, respectively. The red and blue circles represent the donor and acceptor respectively.

In comparison with the EF_{th} in the perfect cavity, the EF_{th} in the silver cavity shows the similar interference patterns, but with additional characteristics (**Figure 1c**). Here we set the metal thickness as 35 nm resembling most of the experimental conditions.[36-37] In such a silver cavity, the resonance wavelength changes from the sharp distribution at 500 nm to a broad distribution ranging from 560 to 600 nm. The redshift of the resonance wavelength arises from the skin effect, and its magnitude is related to the calculated skin depths δ of the silver thin film in the UV/Visible regime (δ = 22 ~ 29 nm) (**Figure S2**). Note that the skin depths in the silver thin film calculated by the FDTD method are similar to the ones found for circular hole arrays drilled in silver thin films at wavelengths over 500 nm.[75] In addition, in the UV/Visible regime, the transmission and absorption of the silver plates further increases the cavity loss, leading to the smaller EF_{th} ~ 2 than in the perfect cavity. Furthermore, the cavity-resonant wavelength strongly depends on the dielectric constant of the medium between the two metal plates, which is supported by the redshifted cavity-resonant wavelength (~870 nm) in the medium SiO_2 (**Figure S3**). Similar

phenomenon has been analyzed in metal spheres coated with dielectric mediums (core/shell structure).[58] Moreover, due to the effect of bulk plasmons (~330 nm), the enhancements at 335 nm are higher as the acceptor approaches the metal surface.[76]

In addition to the RET enhancements along the cavity axis, the cavity modes also influence the RET along the direction parallel to the plane,[68, 74] which is elaborated in **Figure 1d-1f**. **Figure 1d** considers RET enhancement when the acceptor moves along the y direction, with **Figure 1e** showing the dependence of EF_{th} on R_y for the perfect cavity, and **Figure 1f** for the silver FP cavity. Both cavities exhibit significant enhancements in the intermediate-field regime due to the contributions from cavity modes. Note that there is no space confinement for the propagating direction of the cavity modes, like waveguide modes. A previous study reported that the coupling factors of the cavity modes have $1/ R_y$ dependence when $kR_y > 1$ (far-field regime),[74] and here we show how this evolves into the near-field. Similar result exhibits in the system with both the transition dipoles of the donor and acceptor aligned along the y direction (**Figure S4**). By contrast, as the transition dipoles of the two molecules and the cavity axis have the same direction, the EF_{th} shows negligible enhancements since the direction of the dipoles is perpendicular to the electric fields of the cavity modes (**Figure S5**). These results reveal that cavity modes can assist RET enhancement along the direction with no space confinement once the dipoles are aligned with the electric fields of cavity modes. In addition, cavity loss for the silver cavity leads to a decrease in EF_{th} and a broadening of the peak in EF_{th} in the 400-600 nm wavelength domain. In comparison with the sharp distribution in the perfect cavity, spectral broadening in the silver cavity may provide a more convenient platform for optimizing the RET enhancement. Here we clearly show that strong RET enhancements cannot occur when two molecules along the cavity axis in a silver cavity, but strong RET enhancements can occur when two molecules along the y axis (**Figure 1d**). Our finding subverts the physical pictures in the previous studies,[36-40, 68] which may provide a key insight in long-range RET.

3.2. Thickness dependence of EF in the silver cavity

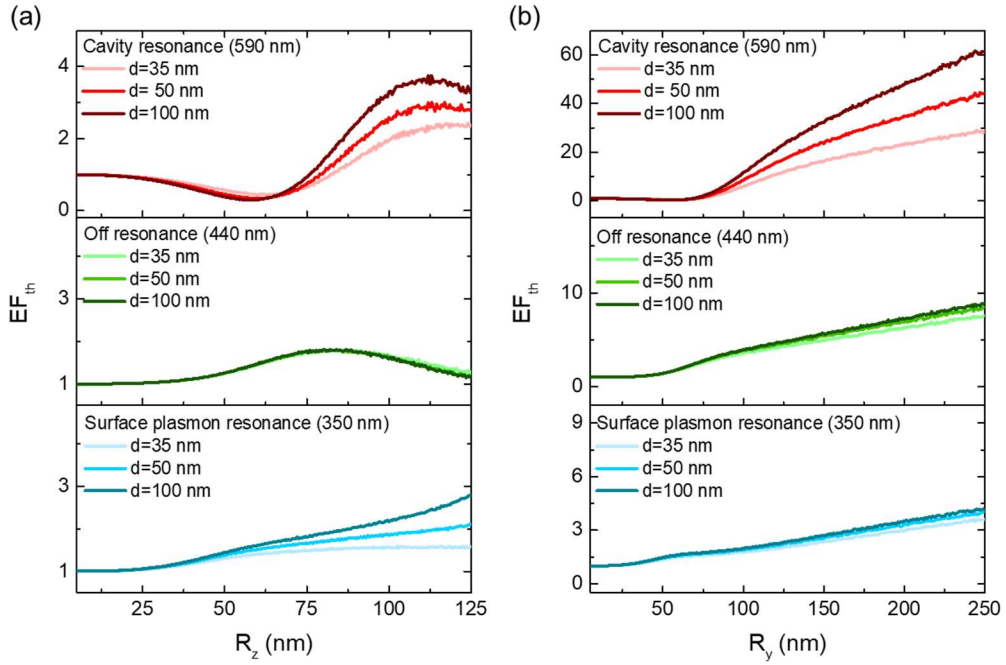

Figure 2. Metal thickness dependence of the EF_{th} in the FP silver cavity with the donor located at the center of the cavity. d denotes the thickness of metal plates. (a) and (b) are the R_z dependence and R_y dependence of enhancement factors respectively.

Tuning metal thickness is a common approach to control the cavity loss in experiments.[77-79] However, almost all studies put emphasis on RET in a perfect cavity, and the effect of cavity loss on RET rates is still unclear. To clarify the effect of cavity loss on RET, we change the metal thickness d from 35 nm to 100 nm (Figure 2) of a silver cavity and explore the metal thickness dependence of the RET enhancements in the silver FP cavity. Based on the wavelength dependence in **Figure 1**, we focused on three types of wavelengths: cavity resonance (590 nm), off resonance (440 nm) and surface plasmon resonance (350 nm) to simplify the discussion. As for the R_z dependence (**Figure 2a**), under the cavity resonance condition and the surface plasmon resonance condition, the EF_{th} slightly increases at long distance (R_z>80 nm) as the metal thickness increases. This could be understood by the fact that the increase in metal thickness can create better confinement for the cavity modes and enhance the silver intraband absorption (which assists RET). According to the weak enhancements in **Figure 2a**, tuning the metal thickness cannot significantly improve RET rates for the donor and acceptor located along the z direction. Note that we chose to

study the enhancement factors instead of the coupling factors because the coupling factors cannot exhibit distinct differences in silver cavities with different thicknesses (**Figure S6**).

As for the R_y dependence (**Figure 2b**), the increase in metal thickness significantly improves the rate enhancement (EF_{th} > 20 at R_y > 100 nm) under the cavity resonance condition because the direction from the donor to acceptor is parallel to the propagating direction of the cavity modes. On the other hand, the increase in metal thickness does not affect the EF_{th} in the plasmon resonance case because the acceptor at the cavity center is far away from the zone of surface plasmon polaritons (SPPs). The other evidence in the plasmon resonance situation is that the EF_{th} is smaller than 4 in **Figure 2**, indicating that the mechanism is not related to SPPs.[59] According to the above results, in spite that the Ry dependence of the EF_{th} in the thicker silver cavity (d = 100 nm) is still far from the one in the perfect cavity, it is no doubt that increasing metal thickness can enhance the RET enhancements along the y axis.

3.3. Influence of the position of the donor in the silver cavity

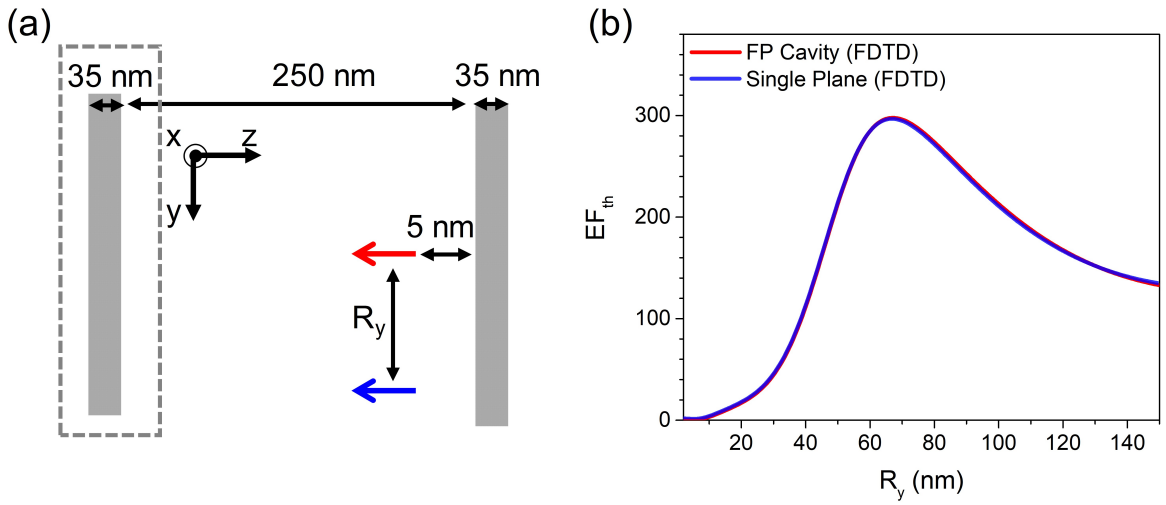

Figure 3. Theoretical RET enhancement (EF_{th}) in the FP silver cavity (d = 35 nm) with the donor near the metal surface (5 nm). (a) The system with the donor (red) and the acceptor (blue) with the displacement along the y direction (R_y). The transition dipoles of the donor and acceptor are located along the z direction. The gray frame denotes the removed silver plate. (b) R_y dependence of the EF_{th} at the wavelength 350 nm (bulk plasmon resonance). The legend "single plane" indicates the system without the framed silver plate.

Previous studies indicate that the highest photonic density of states is located at the center of the cavity according to the phenomenological single-cavity-mode models.[36-37, 80] However, it is crucial to re-examine this concept in the framework of the macroscopic QED, which allows us to consider the effects of infinite photonic modes. In addition, as dipoles are close to the metal surface, the significant plasmonic effect will arise. As a result, it is crucial to elucidate how plasmonic modes together with cavity modes affect the RET enhancements at the same time.

Let us now consider the EF_{th} with the donor shifted from the center by 50 nm along the z direction (75 nm above one of the metal plates). EF_{th} values for the silver FP cavity are presented in **Figure S7**, and it is clear that these show a similar pattern to **Figure 2**. However, as the donor approaches the metal surface (5 nm above one of the metal plates in **Figure 3**) with the transition dipole along the z direction, a significant enhancement $EF_{th} \sim 300$ occurs at $R_y = 65$ nm for a wavelength of 350 nm. Note that we assume that no electron transfer is involved in the RET process. To clarify the origin of the enhancement, we evaluated the EF_{th} in the system without the framed silver plate, which shows almost the same behavior as the one in the cavity (**Figure 3b**). The decrease in EF_{th} for $R_y > 65$ nm arises from destructive interference between the charge antisymmetric and charge symmetric modes of surface plasmons, as has been discussed in a previous report.[59] In addition, the system with both the transition dipoles of the two molecules aligned along the y direction also shows the significant enhancement $EF_{th} \sim 100$ occurs at $R_y = 100$ nm for a wavelength of 350 nm (**Figure S8**). Due to the contribution of the cavity modes (**Figure S4**), the enhancements in the FP cavity are slightly higher than the ones above a single silver plane. The results, together with the resonance wavelength verifies that the enhancements are not majorly relevant to the cavity modes but to the SPPs. The overlap of the EF in the cavity and above a single plate reveals that the enhancements caused by the SPPs are much stronger than those caused by the cavity modes. According to **Figure 2b** and **3b**, significant long-range energy transfer can be achieved through the cavity modes or the surface plasmon polariton modes.

It is interesting to summarize the results presented so far in terms of concepts that are associated with H and J molecular aggregates. Here we use "H/J dimer" to represent the side-by-side/head-to-tail alignments of the transition dipoles. Based on the above results for the FP silver cavity, the RET enhancements are summarized in **Scheme 2**. First, when the displacement vector between the two molecules is aligned with the cavity axis (H-1 and J-1), the cavity modes cannot

give strong RET enhancement (EF_{th} < 10) due either to interference between resonant and non-resonant cavity modes (H-1 case) or to the orthogonality of the transition dipoles and the electric fields of the cavity modes (J-1 case). Second, when the displacement vector between the two molecules is perpendicular to the cavity axis, the large RET enhancements can occur (H-2 and J-2) for those cavity modes whose electric fields are aligned with the transition dipoles. Third, if the dimer is near the metal surface (within the range of the SPPs), the surface plasmon modes can render significant RET enhancements (H-4 and J-3). This information is beneficial to experimental designs to realize long-range RET in FP cavities.

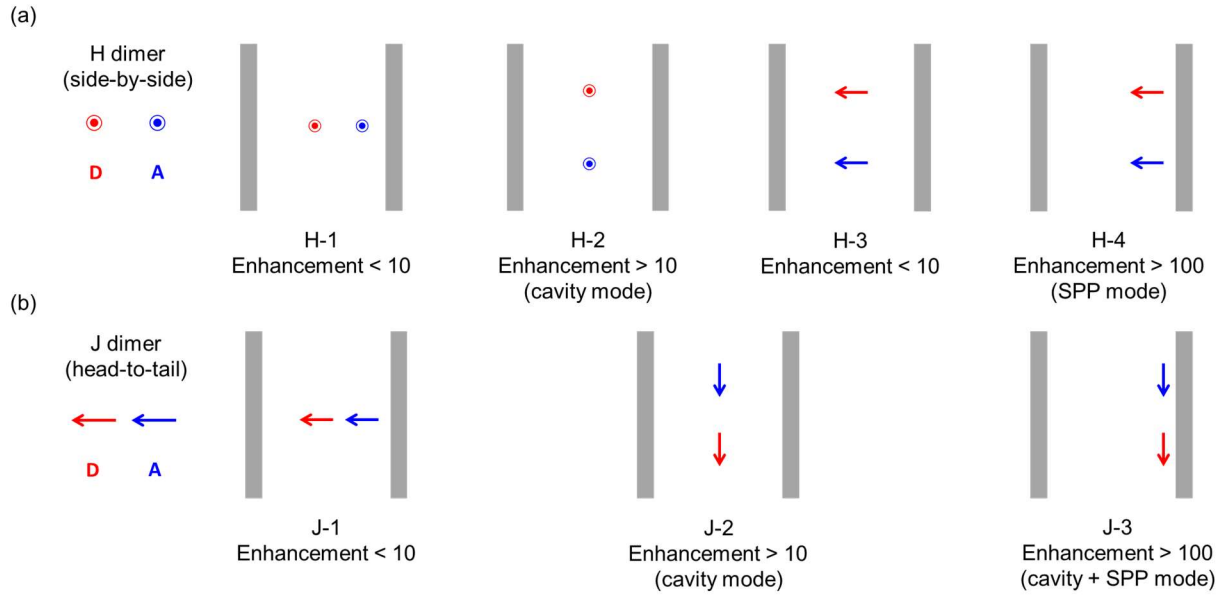

Scheme 2. Summarized RET enhancement in the silver FP cavity. (a) The system with the donor (red) and the acceptor (blue) with the side-by-side alignment (H dimer). The labels "◉" indicate the direction outward from the plane of the figure. H-1 and H-2 correspond to the results in **Figure 1**. H-3 denotes the result in **Figure S5d-5f**. H-4 represents the result in **Figure 3**. (b) The system with the donor (red) and the acceptor (blue) with the head-by-tail alignment (J dimer). J-1 corresponds to the result in **Figure S5a-5c**. J-2 represents the result in **Figure S4**. J-3 denotes the results in **Figure S8**.

3.4. EF in a square silver cavity

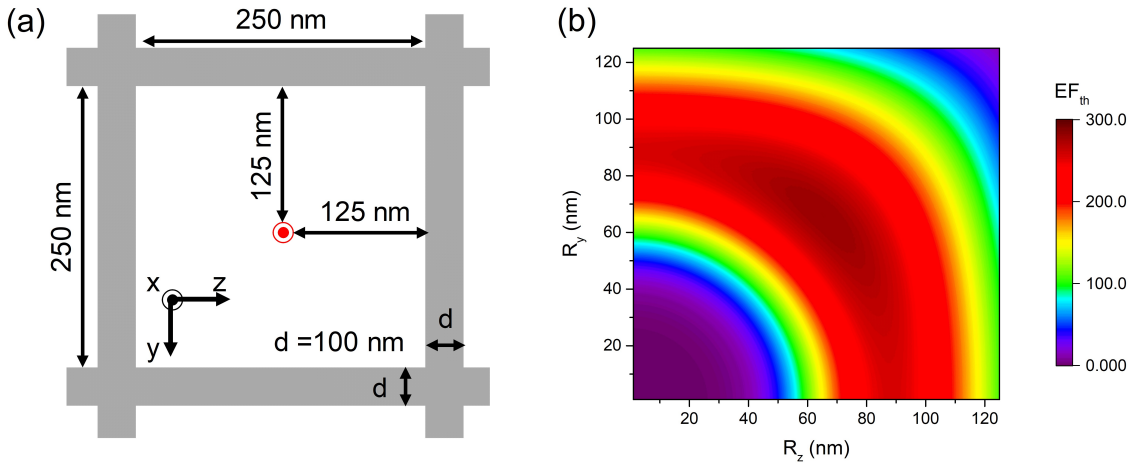

Figure 4. Theoretical RET enhancement (EF_{th}) in the square cavity with the donor located at the center of the cavity with the metal thickness d = 100 nm. (a) The structure of the 2D cavity with the transition dipole of the donor along the x direction. (b) Spatial dependence of the EF_{th} under cavity resonance (λ= 427 nm). The origin is set at the center of the square cavity.

How to design photonic structures to control light-matter interactions is a key concept in nano optics. To demonstrate RET can be significantly changed via material structure designs, we take a square silver cavity as an example, as shown in **Figure 4a**. Here we chose the metal thickness as 100 nm for effective confinement. With these settings, the spatial distribution of the EF_{th} in the first quadrant of the yz plane is presented in **Figure 4b**, showing a remarkable EF_{th} ~ 280 at the location (R_z, R_y) ~ (65 nm, 65 nm) at the wavelength of cavity resonance (λ= 427 nm). This applies to both the H-1 and H-2 cases from Scheme 2, as they are rendered equivalent by the cavity design. Note that the electric field associated with the cavity modes in this case is always in the x direction, so the only J-dimer case that would have significant enhancement would occur when the dipole directions are along x. The resonance wavelength has been examined through a wavelength scan of EF_{th} with the acceptor at (R_z, R_y) = (65 nm, 65 nm) under a wavelength resolution of 0.25 nm (**Figure S9**). Note that the inversion symmetry of the square FP silver cavity (the origin at the center of the square cavity) leads to the same result for EF_{th} in other quadrants. Intriguingly, the additional confinement increases the energy of the cavity mode and results in a blueshift of the cavity resonance wavelength compared with that in the FP cavity. In addition, to verify whether the enhancements arise from the cavity resonance, we removed one of the plates of

the rectangular cavity, and the EF_{th} returns to the behavior in the FP silver cavity (**Figure S10**), i.e., the EF_{th} enhancement by the confinement is associated with the cavity mode. Our simulations validate that RET can be significantly enhanced by cavity modes in a square silver cavity. In addition, this result reveals that the FP cavity is not the only choice to modulate the long-range RET rate. Moreover, through our approach based on the framework of macroscopic QED together with the FDTD numerical simulation, it is feasible to achieve strong RET enhancements via theoretical photonic designs before carrying out experiments.

4. Conclusion

In this study, we have investigated RET enhancements in nanocavities using the generalized RET theory combined with the FDTD method. The main findings can be summarized as follows. First, when the displacement vector between the two H-dimer molecules is aligned with the cavity axis (the normal direction to the surface of the FP silver cavity), interference between resonant and non-resonant cavity modes causes weak energy transfer, with $EF_{th} < 10$, and rate suppression in the FP cavities. In addition, for the same alignment, increase in metal thicknesses or moving of the donor position cannot significantly improve EF_{th}. Suppression of energy transfer is also found for the J-dimer case, because the dipoles are perpendicular to the cavity field. Second, when the displacement vector between the two H-dimer or J-dimer molecules is perpendicular to the cavity axis, the cavity modes can result in large RET enhancement in the system as shown in some cases, and the surface plasmon polariton modes engender significant RET enhancements if the molecules are in close proximity to the surface. Third, the square FP silver cavity seems to be one of the solutions for significantly enhancing long-range energy transfer. Here we first demonstrate how cavity modes and plasmonic modes influence the RET enhancements in the UV-Vis regime in the silver cavities (highly dispersive and absorbing, i.e., realistic cavities). In addition, we provide a simple but clear approach to simulate the RET behaviors resembling real systems, which paves ways for experimentalists to design dielectric environments to achieve highly efficient long-range RET.

Our simulations are reliable because the experimental results together with the analytical solutions to the perfect cavity[28, 68] are consistent with numerical solutions done here based on the FDTD method (**Figure S11**). In addition to the system of perfect cavities, our previous study[48] has

shown that, for the light-matter coupling strength in plasmonic nanocavities, the coupling strength given by our theory is quantitatively in agreement with the experimental results from Cavendish Laboratory.[81] Hence, we believe that the scientific value of this work far exceeds the previous theoretical models using perturbation expansion and cavity QED considering single cavity mode only because we can describe both multiple cavity modes and plasmon polariton modes at the same time. Note that our study only clarifies the RET processes with one pair of donor/acceptor in the nanocavity. In other words, collective RET effects in molecular ensembles or molecular aggregates are not considered here,[39] and this effect deserves further exploration. In addition, this study does not cover RET processes involving polariton formation for the initial state (strong light-matter coupling),[27, 36-37, 39] which is also a key issue concerning RET. Moreover, since the light-matter coupling is proportional to the square root of the number of molecules,[82-83] it is easier for molecular aggregates to achieve strong light-matter interaction and form molecular polaritons than for isolated molecules. To investigate this collective RET effect and establish the theory of RET for strongly coupled molecular aggregates will require additional work, but the present study provides important steps toward solving these tangled issues.

Associated Content

Supporting information

The following files are available free of charge.

Relationship between EF_{th} and EF_{exp}, analysis of the RET in the perfect FP cavity, skin depths of silver thin film, Influence of the dielectric medium in the RET enhancement in a FP cavity. RET enhancement in a FP cavity with shifted position of donor, different dipole alignments and directions of displacement vectors, coupling factor in a silver FP cavity with different metal thickness, wavelength scan of the EF_{th} for the rectangular silver cavity with the acceptor at (Rz, Ry) = (65 nm, 65 nm), RET enhancement in the rectangular silver cavity without one silver, comparison of the EF_{th} between the FDTD method and the analytical solution in a perfect cavity where $kR = 1$.

Acknowledgments

YCW and LYH thank Academia Sinica and the Ministry of Science and Technology of Taiwan (MOST 109-2113-M-001-021, MOST 110-2113-M-001-053) for generous supports. GCS was supported by NSF Grant CHE-2055565. GDS acknowledges funding from the U.S. Department of Energy, Office of Science, Office of Basic Energy Sciences, under Award No. DE-SC0015429.

REFERENCES

1. Nantalaksakul, A.; Reddy, D. R.; Bardeen, C. J.; Thayumanavan, S. Light Harvesting Dendrimers. *Photosynth. Res.* **2006,** *87*, 133-150.
2. Scholes, G. D.; Fleming, G. R.; Olaya-Castro, A.; van Grondelle, R. Lessons from nature about solar light harvesting. *Nat. Chem.* **2011,** *3*, 763-774.
3. Nabiev, I.; Rakovich, A.; Sukhanova, A.; Lukashev, E.; Zagidullin, V.; Pachenko, V.; Rakovich, Y. P.; Donegan, J. F.; Rubin, A. B.; Govorov, A. O. Fluorescent Quantum Dots as Artificial Antennas for Enhanced Light Harvesting and Energy Transfer to Photosynthetic Reaction Centers. *Angew. Chem. Int. Ed.* **2010,** *49*, 7217-7221.
4. Scholes, G. D.; Fleming, G. R. On the Mechanism of Light Harvesting in Photosynthetic Purple Bacteria: B800 to B850 Energy Transfer. *J. Phys. Chem. B* **2000,** *104*, 1854-1868.
5. Scholes, G. D.; Jordanides, X. J.; Fleming, G. R. Adapting the Förster Theory of Energy Transfer for Modeling Dynamics in Aggregated Molecular Assemblies. *J. Phys. Chem. B* **2001,** *105*, 1640-1651.
6. Scholes, G. D.; Curutchet, C.; Mennucci, B.; Cammi, R.; Tomasi, J. How Solvent Controls Electronic Energy Transfer and Light Harvesting. *J. Phys. Chem. B* **2007,** *111*, 6978-6982.
7. Curutchet, C.; Scholes, G. D.; Mennucci, B.; Cammi, R. How Solvent Controls Electronic Energy Transfer and Light Harvesting: Toward a Quantum-Mechanical Description of Reaction Field and Screening Effects. *J. Phys. Chem. B* **2007,** *111*, 13253-13265.
8. Brédas, J.-L.; Sargent, E. H.; Scholes, G. D. Photovoltaic concepts inspired by coherence effects in photosynthetic systems. *Nat. Mater* **2017,** *16*, 35-44.
9. Liu, J.; Mantell, J.; Di Bartolo, N.; Jones, M. R. Mechanisms of Self-Assembly and Energy Harvesting in Tuneable Conjugates of Quantum Dots and Engineered Photovoltaic Proteins. *Small* **2019,** *15*, 1804267.
10. Steiner, A. M.; Lissel, F.; Fery, A.; Lauth, J.; Scheele, M. Prospects of Coupled Organic–Inorganic Nanostructures for Charge and Energy Transfer Applications. *Angew. Chem. Int. Ed.* **2021,** *60*, 1152-1175.
11. Willets, K. A.; Van Duyne, R. P. Localized Surface Plasmon Resonance Spectroscopy and Sensing. *Annu. Rev. Phys. Chem.* **2007,** *58*, 267-297.
12. Langer, J.; Jimenez de Aberasturi, D.; Aizpurua, J.; Alvarez-Puebla, R. A.; Auguié, B.; Baumberg, J. J.; Bazan, G. C.; Bell, S. E. J.; Boisen, A.; Brolo, A. G.; Choo, J.; Cialla-May, D.; Deckert, V.; Fabris, L.; Faulds, K.; García de Abajo, F. J.; Goodacre, R.; Graham, D.; Haes, A. J.; Haynes, C. L.; Huck, C.; Itoh, T.; Käll, M.; Kneipp, J.; Kotov, N. A.; Kuang, H.; Le Ru, E. C.; Lee, H. K.; Li, J.-F.; Ling, X. Y.; Maier, S. A.; Mayerhöfer, T.; Moskovits, M.; Murakoshi, K.; Nam, J.-M.; Nie, S.; Ozaki, Y.; Pastoriza-Santos, I.; Perez-Juste, J.; Popp, J.; Pucci, A.; Reich, S.;

Ren, B.; Schatz, G. C.; Shegai, T.; Schlücker, S.; Tay, L.-L.; Thomas, K. G.; Tian, Z.-Q.; Van Duyne, R. P.; Vo-Dinh, T.; Wang, Y.; Willets, K. A.; Xu, C.; Xu, H.; Xu, Y.; Yamamoto, Y. S.; Zhao, B.; Liz-Marzán, L. M. Present and Future of Surface-Enhanced Raman Scattering. *ACS Nano* **2020,** *14*, 28-117.
13. Hildebrandt, N.; Spillmann, C. M.; Algar, W. R.; Pons, T.; Stewart, M. H.; Oh, E.; Susumu, K.; Díaz, S. A.; Delehanty, J. B.; Medintz, I. L. Energy Transfer with Semiconductor Quantum Dot Bioconjugates: A Versatile Platform for Biosensing, Energy Harvesting, and Other Developing Applications. *Chem. Rev.* **2017,** *117*, 536-711.
14. Geißler, D.; Stufler, S.; Löhmannsröben, H.-G.; Hildebrandt, N. Six-Color Time-Resolved Förster Resonance Energy Transfer for Ultrasensitive Multiplexed Biosensing. *J. Am. Chem. Soc.* **2013,** *135*, 1102-1109.
15. Scholes, G. D. Long-Range Resonance Energy Transfer in Molecular Systems. *Annu. Rev. Phys. Chem.* **2003,** *54*, 57-87.
16. Jones, G. A.; Bradshaw, D. S. Resonance Energy Transfer: From Fundamental Theory to Recent Applications. *Front. Phys.* **2019,** *7*.
17. Andrews, D. L.; Bradshaw, D. S. Virtual photons, dipole fields and energy transfer: a quantum electrodynamical approach. *Eur. J. Phys.* **2004,** *25*, 845-858.
18. Juzeliūnas, G.; Andrews, D. L. Quantum electrodynamics of resonant energy transfer in condensed matter. *Phys. Rev. B* **1994,** *49*, 8751-8763.
19. Daniels, G. J.; Jenkins, R. D.; Bradshaw, D. S.; Andrews, D. L. Resonance energy transfer: The unified theory revisited. *J. Chem. Phys.* **2003,** *119*, 2264-2274.
20. Ford, J. S.; Salam, A.; Jones, G. A. A Quantum Electrodynamics Description of Quantum Coherence and Damping in Condensed-Phase Energy Transfer. *J. Phys. Chem. Lett.* **2019,** *10*, 5654-5661.
21. Salam, A. A general formula for the rate of resonant transfer of energy between two electric multipole moments of arbitrary order using molecular quantum electrodynamics. *J. Chem. Phys.* **2005,** *122*, 044112.
22. Martín-Cano, D.; Martín-Moreno, L.; García-Vidal, F. J.; Moreno, E. Resonance Energy Transfer and Superradiance Mediated by Plasmonic Nanowaveguides. *Nano Lett.* **2010,** *10*, 3129-3134.
23. Poudel, A.; Chen, X.; Ratner, M. A. Enhancement of Resonant Energy Transfer Due to an Evanescent Wave from the Metal. *J. Phys. Chem. Lett.* **2016,** *7*, 955-960.
24. Choi, Y.; Park, Y.; Kang, T.; Lee, L. P. Selective and sensitive detection of metal ions by plasmonic resonance energy transfer-based nanospectroscopy. *Nat. Nanotechnol* **2009,** *4*, 742-746.
25. Lunz, M.; Gerard, V. A.; Gun'ko, Y. K.; Lesnyak, V.; Gaponik, N.; Susha, A. S.; Rogach, A. L.; Bradley, A. L. Surface Plasmon Enhanced Energy Transfer between Donor and Acceptor CdTe Nanocrystal Quantum Dot Monolayers. *Nano Lett.* **2011,** *11*, 3341-3345.
26. Garfield, D. J.; Borys, N. J.; Hamed, S. M.; Torquato, N. A.; Tajon, C. A.; Tian, B.; Shevitski, B.; Barnard, E. S.; Suh, Y. D.; Aloni, S.; Neaton, J. B.; Chan, E. M.; Cohen, B. E.; Schuck, P. J. Enrichment of molecular antenna triplets amplifies upconverting nanoparticle emission. *Nat. Photon.* **2018,** *12*, 402-407.
27. Dunkelberger, A. D.; Spann, B. T.; Fears, K. P.; Simpkins, B. S.; Owrutsky, J. C. Modified relaxation dynamics and coherent energy exchange in coupled vibration-cavity polaritons. *Nat. Commun.* **2016,** *7*, 13504.
28. Rustomji, K.; Dubois, M.; Jomin, P.; Enoch, S.; Wenger, J.; de Sterke, C. M.; Abdeddaim, R. Complete Electromagnetic Dyadic Green Function Characterization in a Complex

Environment---Resonant Dipole-Dipole Interaction and Cooperative Effects. *Phys. Rev. X* **2021,** *11*, 021004.
29. Rustomji, K.; Dubois, M.; Kuhlmey, B.; de Sterke, C. M.; Enoch, S.; Abdeddaim, R.; Wenger, J. Direct Imaging of the Energy-Transfer Enhancement between Two Dipoles in a Photonic Cavity. *Phys. Rev. X* **2019,** *9*, 011041.
30. Yang, X.; Li, Y.; Lou, Z.; Chen, Q.; Li, B. Optical Energy Transfer from Photonic Nanowire to Plasmonic Nanowire. *ACS Appl. Energy Mater.* **2018,** *1*, 278-283.
31. Yu, J.; Sharma, M.; Delikanli, S.; Birowosuto, M. D.; Demir, H. V.; Dang, C. Mutual Energy Transfer in a Binary Colloidal Quantum Well Complex. *J. Phys. Chem. Lett.* **2019,** *10*, 5193-5199.
32. Hernández-Martínez, P. L.; Govorov, A. O. Exciton energy transfer between nanoparticles and nanowires. *Phys. Rev. B* **2008,** *78*, 035314.
33. Peters, C. H.; Guichard, A. R.; Hryciw, A. C.; Brongersma, M. L.; McGehee, M. D. Energy transfer in nanowire solar cells with photon-harvesting shells. *J. Appl. Phys.* **2009,** *105*, 124509.
34. Roth, D. J.; Nasir, M. E.; Ginzburg, P.; Wang, P.; Le Marois, A.; Suhling, K.; Richards, D.; Zayats, A. V. Förster Resonance Energy Transfer inside Hyperbolic Metamaterials. *ACS Photonics* **2018,** *5*, 4594-4603.
35. Andrew, P.; Barnes, W. L. Förster Energy Transfer in an Optical Microcavity. *Science* **2000,** *290*, 785-788.
36. Zhong, X.; Chervy, T.; Zhang, L.; Thomas, A.; George, J.; Genet, C.; Hutchison, J. A.; Ebbesen, T. W. Energy Transfer between Spatially Separated Entangled Molecules. *Angew. Chem. Int. Ed.* **2017,** *56*, 9034-9038.
37. Zhong, X.; Chervy, T.; Wang, S.; George, J.; Thomas, A.; Hutchison, J. A.; Devaux, E.; Genet, C.; Ebbesen, T. W. Non-Radiative Energy Transfer Mediated by Hybrid Light-Matter States. *Angew. Chem. Int. Ed.* **2016,** *55*, 6202-6206.
38. Schäfer, C.; Ruggenthaler, M.; Appel, H.; Rubio, A. Modification of excitation and charge transfer in cavity quantum-electrodynamical chemistry. *Proc. Natl. Acad. Sci. U.S.A.* **2019,** *116*, 4883.
39. Du, M.; Martínez-Martínez, L. A.; Ribeiro, R. F.; Hu, Z.; Menon, V. M.; Yuen-Zhou, J. Theory for polariton-assisted remote energy transfer. *Chem. Sci.* **2018,** *9*, 6659-6669.
40. Du, M.; Ribeiro, R. F.; Yuen-Zhou, J. Remote Control of Chemistry in Optical Cavities. *Chem* **2019,** *5*, 1167-1181.
41. Green, D.; Jones, G. A.; Salam, A. Polariton mediated resonance energy transfer in a fluid. *J. Chem. Phys.* **2020,** *153*, 034111.
42. Weeraddana, D.; Premaratne, M.; Gunapala, S. D.; Andrews, D. L. Controlling resonance energy transfer in nanostructure emitters by positioning near a mirror. *J. Chem. Phys.* **2017,** *147*, 074117.
43. Andrews, D. L.; Ford, J. S. Resonance energy transfer: Influence of neighboring matter absorbing in the wavelength region of the acceptor. *J. Chem. Phys.* **2013,** *139*, 014107.
44. Dung, H. T.; Knöll, L.; Welsch, D.-G. Intermolecular energy transfer in the presence of dispersing and absorbing media. *Phys. Rev. A* **2002,** *65*, 043813.
45. Scheel, S.; Buhmann, S. Y. Macroscopic QED - Concepts and Applications. *arXiv* **2009**, 0902.3586.
46. Wang, S.; Lee, M.-W.; Chuang, Y.-T.; Scholes, G. D.; Hsu, L.-Y. Theory of molecular emission power spectra. I. Macroscopic quantum electrodynamics formalism. *J. Chem. Phys.* **2020,** *153*, 184102.

47. Wang, S.; Scholes, G. D.; Hsu, L.-Y. Coherent-to-Incoherent Transition of Molecular Fluorescence Controlled by Surface Plasmon Polaritons. *J. Phys. Chem. Lett.* **2020,** *11*, 5948-5955.
48. Wang, S.; Scholes, G. D.; Hsu, L.-Y. Quantum dynamics of a molecular emitter strongly coupled with surface plasmon polaritons: A macroscopic quantum electrodynamics approach. *J. Chem. Phys.* **2019,** *151*, 014105.
49. Dung, H. T.; Knöll, L.; Welsch, D.-G. Spontaneous decay in the presence of dispersing and absorbing bodies: General theory and application to a spherical cavity. *Phys. Rev. A* **2000,** *62*, 053804.
50. Raabe, C.; Scheel, S.; Welsch, D.-G. Unified approach to QED in arbitrary linear media. *Phys. Rev. A* **2007,** *75*, 053813.
51. Dung, H. T.; Buhmann, S. Y.; Knöll, L.; Welsch, D.-G.; Scheel, S.; Kästel, J. Electromagnetic-field quantization and spontaneous decay in left-handed media. *Phys. Rev. A* **2003,** *68*, 043816.
52. Dung, H. T.; Knöll, L.; Welsch, D.-G. Resonant dipole-dipole interaction in the presence of dispersing and absorbing surroundings. *Phys. Rev. A* **2002,** *66*, 063810.
53. Jauch, J. M.; Watson, K. M. Phenomenological Quantum-Electrodynamics. *Phys. Rev.* **1948,** *74*, 950-957.
54. Watson, K. M.; Jauch, J. M. Phenomenological Quantum Electrodynamics. Part III. Dispersion. *Phys. Rev.* **1949,** *75*, 1249-1261.
55. Huttner, B.; Barnett, S. M. Quantization of the electromagnetic field in dielectrics. *Phys. Rev. A* **1992,** *46*, 4306-4322.
56. Hopfield, J. J. Theory of the Contribution of Excitons to the Complex Dielectric Constant of Crystals. *Phys. Rev.* **1958,** *112*, 1555-1567.
57. Dung, H. T.; Knöll, L.; Welsch, D.-G. Three-dimensional quantization of the electromagnetic field in dispersive and absorbing inhomogeneous dielectrics. *Phys. Rev. A* **1998,** *57*, 3931-3942.
58. Lee, M.-W.; Hsu, L.-Y. Controllable Frequency Dependence of Resonance Energy Transfer Coupled with Localized Surface Plasmon Polaritons. *J. Phys. Chem. Lett.* **2020,** *11*, 6796-6804.
59. Wu, J.-S.; Lin, Y.-C.; Sheu, Y.-L.; Hsu, L.-Y. Characteristic Distance of Resonance Energy Transfer Coupled with Surface Plasmon Polaritons. *J. Phys. Chem. Lett.* **2018,** *9*, 7032-7039.
60. Ding, W.; Hsu, L.-Y.; Heaps, C. W.; Schatz, G. C. Plasmon-Coupled Resonance Energy Transfer II: Exploring the Peaks and Dips in the Electromagnetic Coupling Factor. *J. Phys. Chem. C* **2018,** *122*, 22650-22659.
61. Hsu, L.-Y.; Ding, W.; Schatz, G. C. Plasmon-Coupled Resonance Energy Transfer. *J. Phys. Chem. Lett.* **2017,** *8*, 2357-2367.
62. Ding, W.; Hsu, L.-Y.; Schatz, G. C. Plasmon-coupled resonance energy transfer: A real-time electrodynamics approach. *J. Chem. Phys.* **2017,** *146*, 064109.
63. Hopmeier, M.; Guss, W.; Deussen, M.; Göbel, E. O.; Mahrt, R. F. Enhanced Dipole-Dipole Interaction in a Polymer Microcavity. *Phys. Rev. Lett.* **1999,** *82*, 4118-4121.
64. Johnson, P. B.; Christy, R. W. Optical Constants of the Noble Metals. *Phys. Rev. B* **1972,** *6*, 4370-4379.
65. Palik, E. D. *Handbook of optical constants of solids*. Academic Press: Orlando, 1985.
66. Baroni, S.; Resta, R. Ab initio calculation of the macroscopic dielectric constant in silicon. *Phys. Rev. B* **1986,** *33*, 7017-7021.

67. Cossi, M.; Barone, V.; Mennucci, B.; Tomasi, J. Ab initio study of ionic solutions by a polarizable continuum dielectric model. *Chem. Phys. Lett.* **1998,** *286*, 253-260.
68. Kobayashi, T.; Zheng, Q.; Sekiguchi, T. Resonant dipole-dipole interaction in a cavity. *Phys. Rev. A* **1995,** *52*, 2835-2846.
69. Förster, T. Zwischenmolekulare Energiewanderung und Fluoreszenz. *Ann. Phys.* **1948,** *437*, 55-75.
70. Knox, R. S.; van Amerongen, H. Refractive Index Dependence of the Förster Resonance Excitation Transfer Rate. *J. Phys. Chem. B* **2002,** *106*, 5289-5293.
71. Novotny, L.; Hecht, B. *Principles of nano-optics*. 2nd ed.; Cambridge University Press: Cambridge, 2012.
72. Jackson, J. D. *Classical electrodynamics*. 3rd ed.; Wiley: New York, 1999.
73. Lumerical, Inc., FDTD Solutions. http://www.lumerical.com/tcad-products/fdtd/(accessed 2019-008-15). . .
74. LaCount, M. D.; Lusk, M. T. Electric dipole coupling in optical cavities and its implications for energy transfer, up-conversion, and pooling. *Phys. Rev. A* **2016,** *93*, 063811.
75. Rodrigo, S. G.; García-Vidal, F. J.; Martín-Moreno, L. Influence of material properties on extraordinary optical transmission through hole arrays. *Phys. Rev. B* **2008,** *77*, 075401.
76. Gong, J.; Dai, R.; Wang, Z.; Zhang, Z. Thickness Dispersion of Surface Plasmon of Ag Nano-thin Films: Determination by Ellipsometry Iterated with Transmittance Method. *Sci. Rep.* **2015,** *5*, 9279.
77. Boltasseva, A.; Nikolajsen, T.; Leosson, K.; Kjaer, K.; Larsen, M. S.; Bozhevolnyi, S. I. Integrated optical components utilizing long-range surface plasmon polaritons. *J. Lightwave Technol.* **2005,** *23*, 413-422.
78. Rahman, B. M. A.; Quadir, A.; Tanvir, H.; Grattan, K. T. V. Characterization of Plasmonic Modes in a Low-Loss Dielectric-Coated Hollow Core Rectangular Waveguide at Terahertz Frequency. *IEEE Photonics Journal* **2011,** *3*, 1054-1066.
79. Kim, M. W.; Ku, P.-C. The metal-clad semiconductor nanoring laser and its scaling properties. *Opt. Express* **2011,** *19*, 3218-3225.
80. Ebbesen, T. W. Hybrid Light–Matter States in a Molecular and Material Science Perspective. *Acc. Chem. Res.* **2016,** *49*, 2403-2412.
81. Chikkaraddy, R.; de Nijs, B.; Benz, F.; Barrow, S. J.; Scherman, O. A.; Rosta, E.; Demetriadou, A.; Fox, P.; Hess, O.; Baumberg, J. J. Single-molecule strong coupling at room temperature in plasmonic nanocavities. *Nature* **2016,** *535*, 127-130.
82. Kadyan, A.; Shaji, A.; George, J. Boosting Self-interaction of Molecular Vibrations under Ultrastrong Coupling Condition. *J. Phys. Chem. Lett.* **2021,** *12*, 4313-4318.
83. Lather, J.; Bhatt, P.; Thomas, A.; Ebbesen, T. W.; George, J. Cavity Catalysis by Cooperative Vibrational Strong Coupling of Reactant and Solvent Molecules. *Angew. Chem. Int. Ed.* **2019,** *58*, 10635-10638.